

Supporting Information

Superexchange on the Fast Lane – Intramolecular electron transfer in a molecular triad occurs by conformationally-gated superexchange

Yusen Luo,^{1,2} Maria Wächtler,^{1,2} Kevin Barthelmes,^{3,4} Andreas Winter,^{3,4} Ulrich S. Schubert^{3,4} and Benjamin Dietzek^{*1,2,4}

¹Institute of Physical Chemistry and Abbe Center of Photonics, Friedrich Schiller-University Jena, Helmholtzweg 4, 07743 Jena, Germany

²Department Functional Interfaces, Leibniz Institute of Photonic Technology (IPHT), Albert-Einstein-Straße 9, 07745 Jena, Germany

³Laboratory of Organic and Macromolecular Chemistry (IOMC), Friedrich Schiller-University Jena, Humboldtstraße 10, 07743 Jena, Germany

⁴Center for Energy and Environmental Chemistry Jena (CEEC Jena), Friedrich Schiller-University Jena, Philosophenweg 7a, 07743 Jena, Germany

**Corresponding author: benjamin.dietzek@leibniz-ipht.de*

Experimental details

The synthesis, steady-state emission spectra, electrochemical properties and photoinduced dynamics of **1–3** at room temperature have been reported elsewhere.¹⁻³

Time-Resolved Spectroscopy. Femtosecond (fs) transient absorption (TA) spectra were collected by using a previously reported home-built pump-probe laser system which is based on an amplified Ti: Sapphire oscillator (1 kHz, 800 nm).⁴ Samples were excited by pump pulse centered at 520 nm (TOPAS-C, Lightconversion Ltd.) with a duration of 80 fs. The power of the pump beam at the sample position was kept at 0.35 mW, corresponding to an energy of 0.7 μ J per pump pulse. A white light supercontinuum generated by focusing a fraction of the fundamental in a CaF₂ plate is used to probe the samples in a wide spectral range (340 to 750 nm). The pump beam is delayed in time with respect to the probe beam by means of an optical delay line and the polarization between probe and pump is set at the magic angle (54.7°). For TA spectroscopy the samples are placed in a 1 cm cuvette (with an optical density of 0.24 at the excitation wavelength) which is placed in a temperature-controlled cryostat (Optistat DN, Oxford Instrument) cooled with liquid nitrogen. Temperatures were set by a temperature controller (ITC 503S, Oxford Instruments) and the actual temperature inside the cuvette is monitored by a temperature sensor connected to a digital multimeter (Keithley 2000 multimeter). A fresh solution is used for measurement at each temperature. The fs TA spectra are displayed after chirp correction. The fs TA data were analyzed by a global multi-exponential fit after exclusion of a temporal window of 500 fs around time-zero in order to avoid contributions of the coherent-artifact region to the data analysis. Furthermore, a spectral band of ca. 20 nm around the pump-wavelength is omitted from the data analysis due to pump-scatter in this spectral range. During all experiments the sample integrity was ensured by recording UV/Vis absorption spectra at room temperature before and after each fs TA measurement.

Relaxation scheme of triads upon excitation

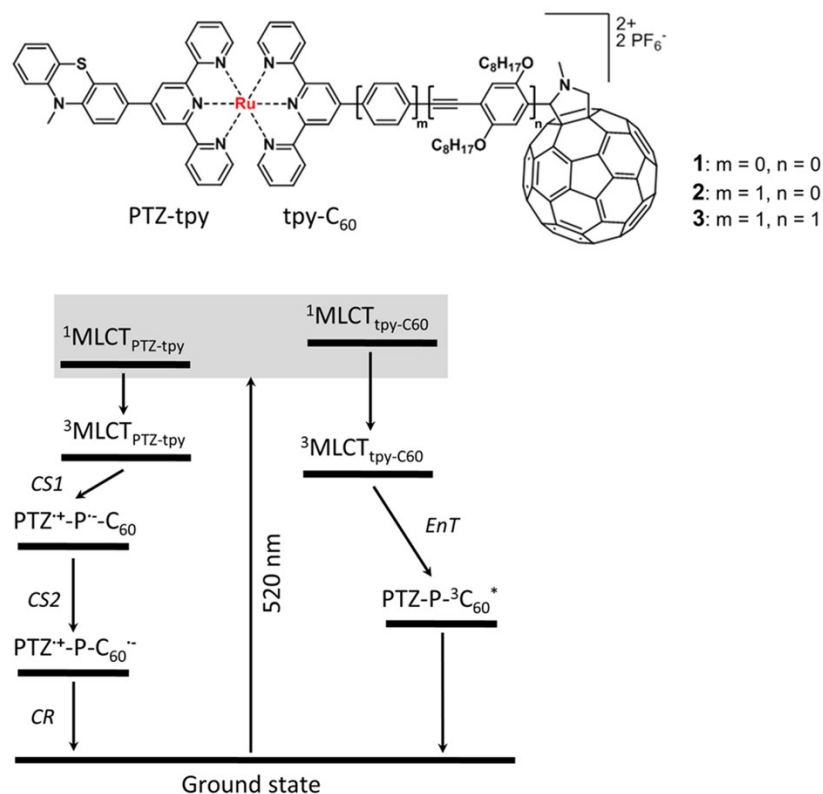


Figure S1. Relaxation processes for **1-3** which refer to the model proposed at room temperature.^{1,2} Terpyridine (tpy) ligand connected with *N*-methylphenothiazine (PTZ) and fullerene (C_{60}) are named as PTZ-tpy and tpy- C_{60} , respectively. Excitation of $\text{Ru}(\text{tpy})_2$ photosensitizer generates two differently distributed MLCT states, *i.e.* $\text{MLCT}_{\text{PTZ-tpy}}$ and $\text{MLCT}_{\text{tpy-C60}}$, which decays *via* electron transfer (left side) and energy transfer (right side), respectively.

Temperature dependent fs TA spectra of **1**

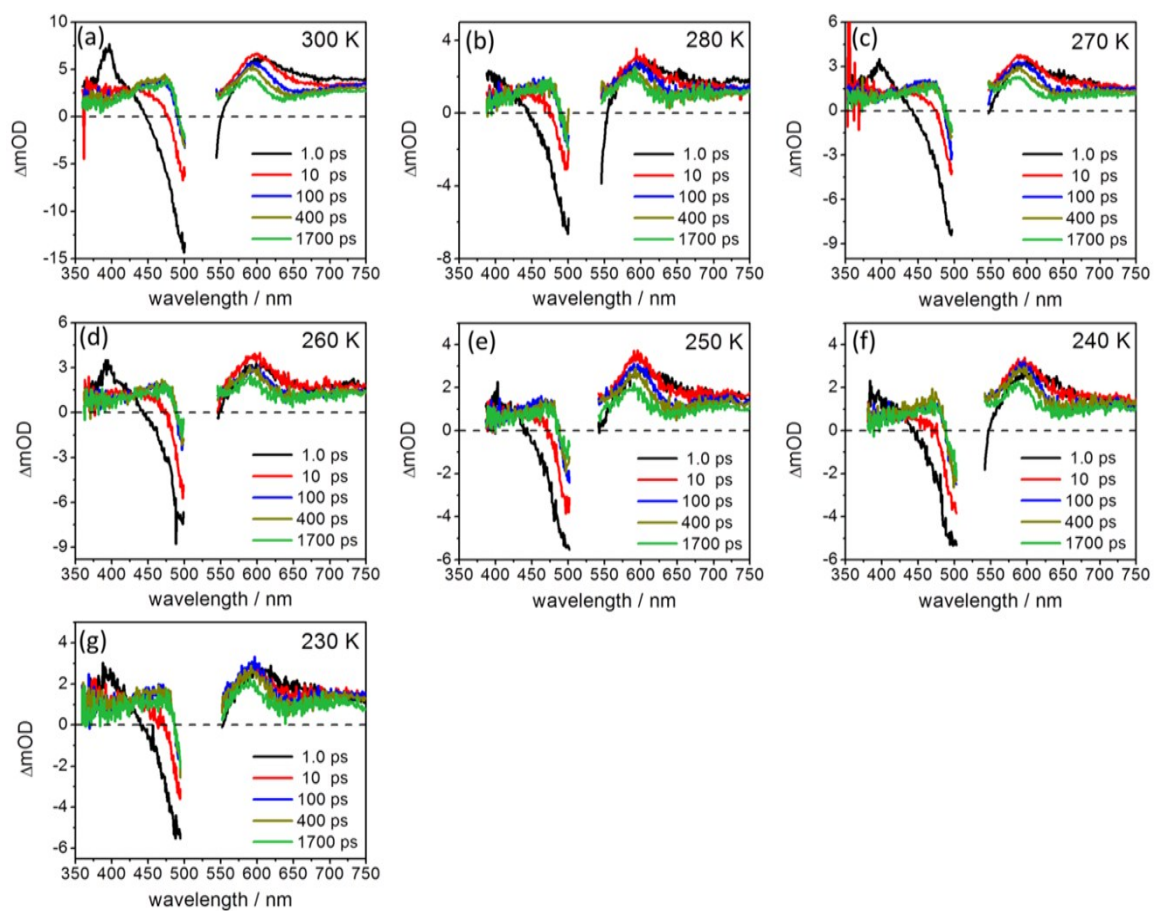


Figure S2. fs transient absorption spectra of **1** upon excitation at 520 nm in dichloromethane at selected delay times at temperature regions from 300 to 230 K.

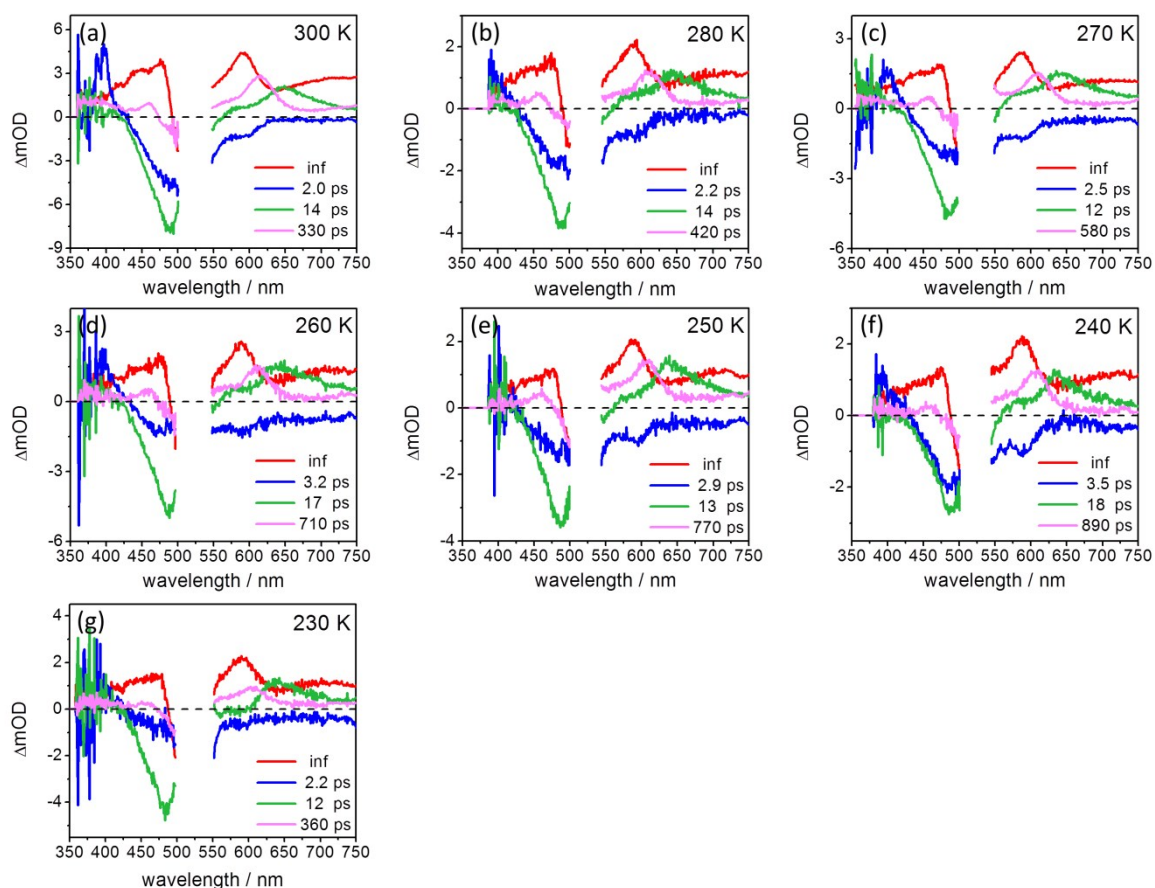


Figure S3. Decay-associated spectra of **1** resulting from the global fit upon excitation at 520 nm in dichloromethane.

We would like to point out that the fs TA data at 230 K (Figure S3g) yields three kinetic processes which are all faster than the corresponding process at higher temperatures. Meanwhile the spectral features of the second and third components in Figure S3g are different to the other data. Thus, the data point of the shortest triad **1** at the lowest temperature 230 K was not included in the Marcus analysis in the main text.

Temperature dependent fs TA spectra of **2**

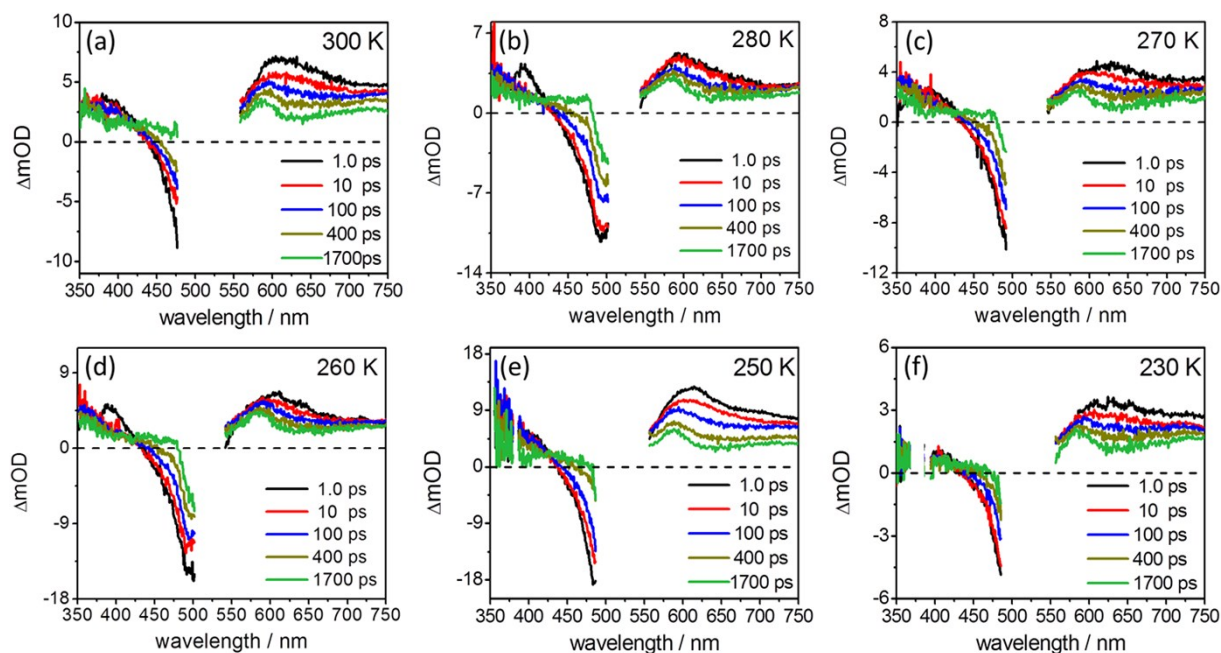


Figure S4. fs transient absorption spectra of **2** upon excitation at 520 nm in dichloromethane at selected delay times at temperature regions from 300 to 230 K.

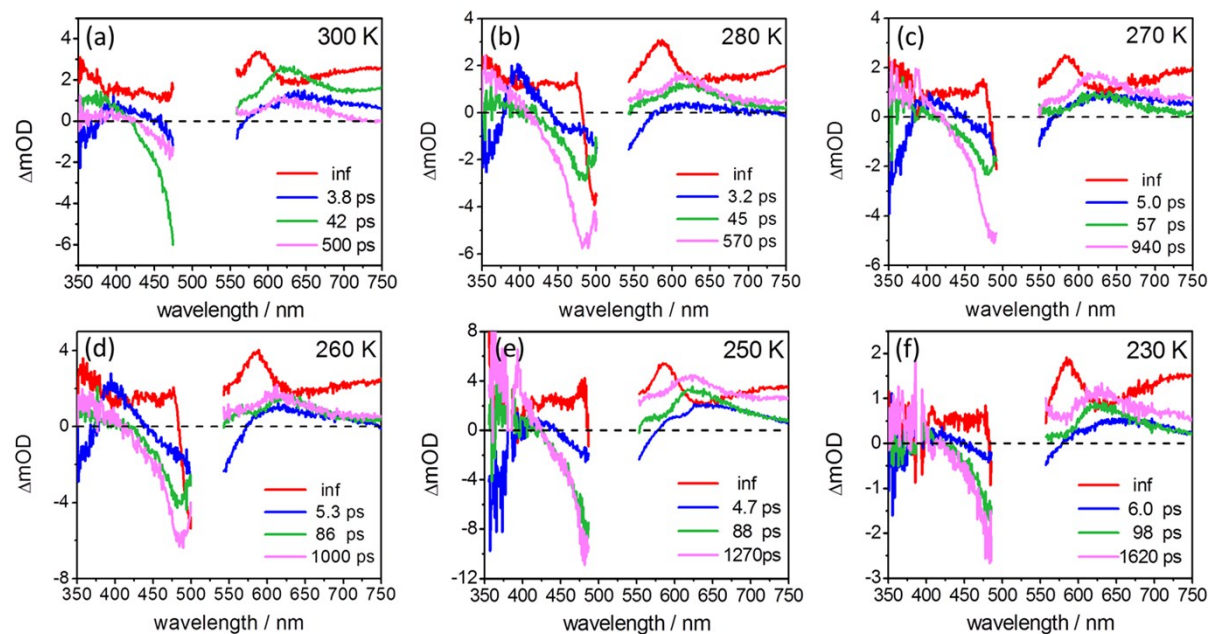


Figure S5. Decay-associated spectra of **2** resulting from the global fit upon excitation at 520 nm in dichloromethane.

Temperature dependent fs TA spectra of **3**

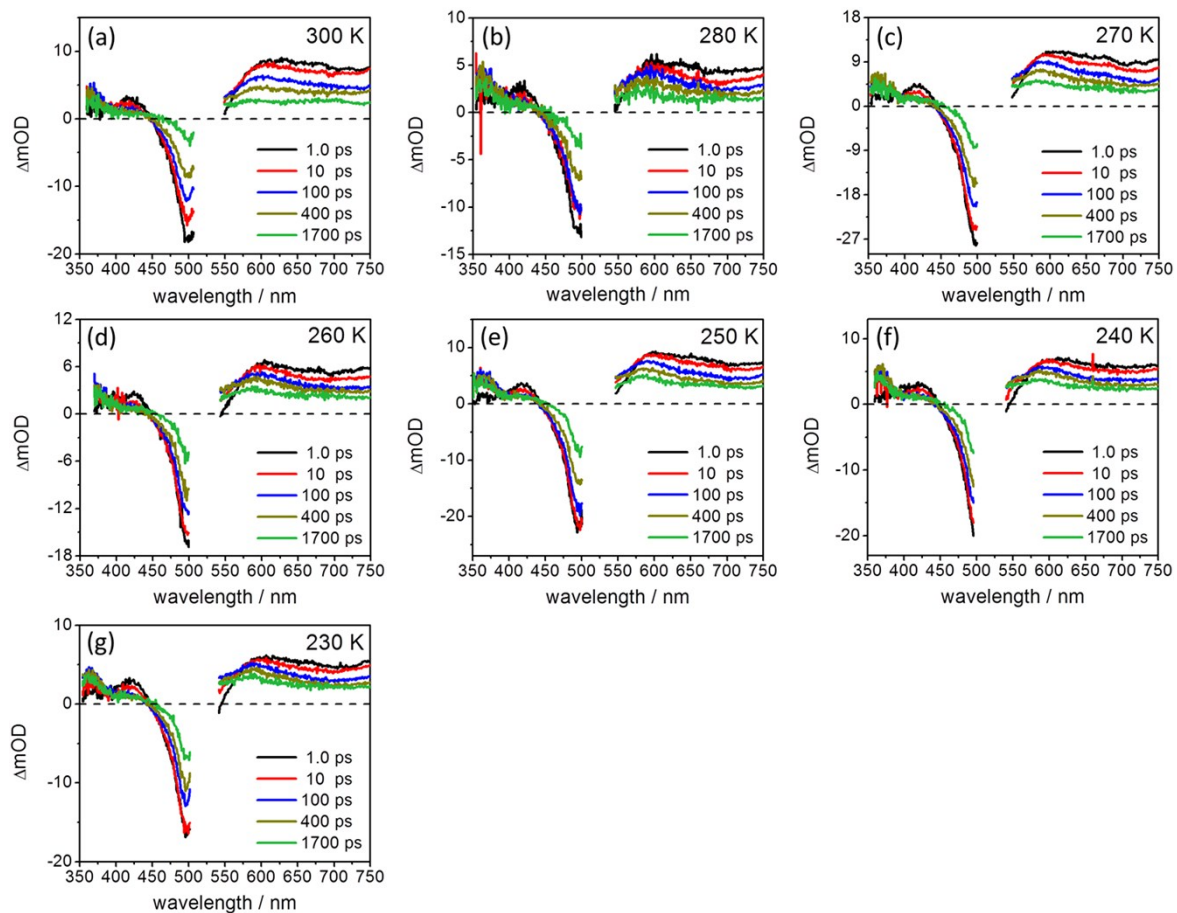


Figure S6. fs transient absorption spectra of **3** upon excitation at 520 nm in dichloromethane at selected delay times at temperature regions from 300 to 230 K.

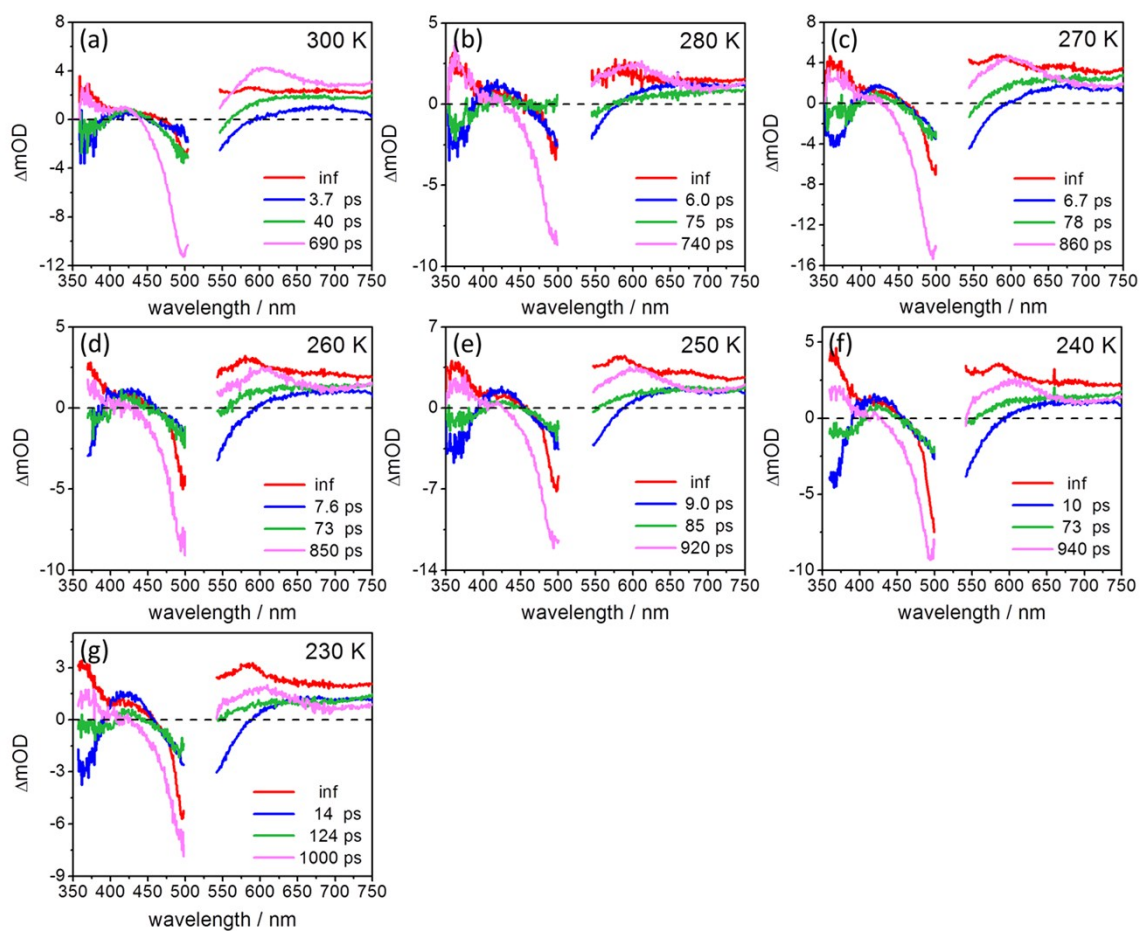


Figure S7. Decay-associated spectra of **3** resulting from the global fit upon excitation at 520 nm in dichloromethane.

Estimation of reorganization energy and the temperature dependence

$$\lambda = \lambda_i + \lambda_o \quad (1)$$

$$\lambda_o = \frac{e^2}{4 \cdot \pi \cdot \epsilon_0} \cdot \left(\frac{1}{2a_1} + \frac{1}{2a_2} - \frac{1}{R_{DA}} \right) \cdot \left(\frac{1}{n^2} - \frac{1}{\epsilon_s} \right) \quad (2)$$

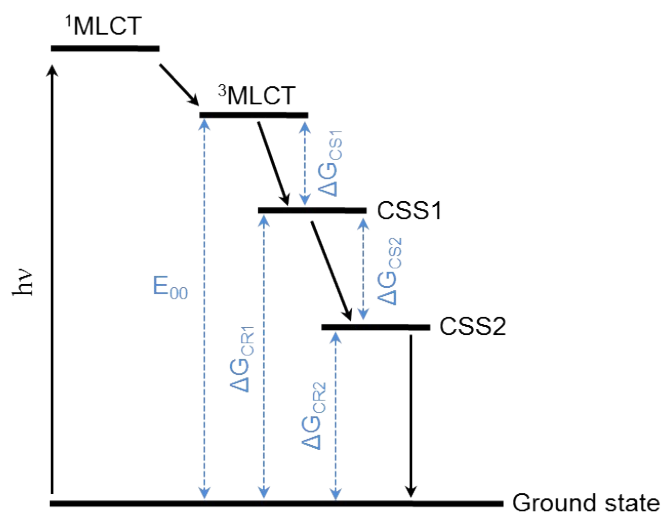
where λ_i and λ_o represent the inner and outer reorganization energy, respectively.⁵ λ_i reflects the free energy change associated with the nuclear bond length changes within molecules while λ_o accounts for the reorganization of the surrounding chemical environment, e.g. solvent molecules. In the simplest model, electron donor and acceptor are treated as spheres with radii a_1 and a_2 .⁶ R_{DA} is the distance between donor and acceptor. n and ϵ_s represent refractive index and dielectric constant of the solvent involved during charge transfer, respectively. ϵ_0 is the vacuum permittivity (8.85×10^{-12} F/m).

For this triad system:

1. λ_i is estimated to be 0.1 eV^{6,7} and commonly treated as distance⁶ and temperature independent.^{8,9}
2. Both n and ϵ_s are temperature dependent, $\epsilon_s(T) = a + bT + cT^2 + dT^3$, for dichloromethane, $a = 0.40452 \times 10^2$, $b = -0.17748 \times 10^0$, $c = 0.23942 \times 10^{-3}$, $d = 0$;¹⁰ for dichloromethane $n(T) = 1.59078 - 5.66 \times 10^{-4} T$.¹¹
3. For the first electron transfer ($PTZ-{}^3P^*-C_{60} \rightarrow PTZ^+-P^--C_{60}$), PTZ and Ru complex are the electron donor ($a_1 = 4 \text{ \AA}$) and acceptor ($a_2 = 5 \text{ \AA}$), respectively. The center-to-center distance R_{DA} is 9.6 \AA . For the second electron transfer ($PTZ^+-P^--C_{60} \rightarrow PTZ^+-P-C_{60}^-$), reduced Ru complex and C_{60} are the electron donor ($a_1 = 5 \text{ \AA}$) and acceptor ($a_2 = 4.5 \text{ \AA}$), respectively. The center-to-center distance R_{DA} is 9.3, 13.4 and 20.8 \AA for **1**, **2** and **3**, respectively. Note: the parameters a_1 , a_2 and R_{DA} were estimated from the neutral, optimized molecular structures.^{2,3}

For *ET1*, due to the same electron donor, electron acceptor and the same donor-acceptor distance, identical reorganization energy will be produced which was already shown in a previous study.¹² The calculated reorganization energy for *ET2* as a function of temperature is summarized in Table S2-4.

Temperature dependence of driving forces



$$\Delta G_{CS1} = e(E_{D^+/D} - E_{A/A^-}) - E_{00} - \frac{e^2}{4\pi\epsilon_0\epsilon R_{DA}} \quad (3)$$

$$\Delta G_{CR1} = -\Delta G_{CS1} - E_{00} \quad (4)$$

For the first electron transfer step, the radical pairs are $\text{tpy}^- / \text{PTZ}^+$; E_{00} is the energy difference between the thermalized, lowest $^3\text{MLCT}$ excited state and ground state of Ru complex. E_{00} is taken to be 2.07 eV.²

For the second electron transfer step the radical pairs are $\text{C}_{60}^- / \text{PTZ}^+$.

$$\Delta G_{CS2} = \Delta G_{CR1} - \Delta G_{CR2} \quad (5)$$

$$\Delta G_{CR2} = e(E_{A/A^-} - E_{D^+/D}) + \frac{e^2}{4\pi\epsilon_0\epsilon R_{DA}} \quad (6)$$

The values of $E_{\text{PTZ}^+/\text{PTZ}}$, $E_{\text{tpy}^-/\text{tpy}}$ and $E_{\text{C}_{60}^-/\text{C}_{60}}$ were taken from ref. 3. The influence of temperature on driving forces is caused by the temperature dependent dielectric constant (ϵ) of dichloromethane.

Summary of time and rate constants for *ET2*

Table S1. Temperature dependence of time constants and the corresponding rate constants for the second electron transfer process in **1–3** obtained from the global fit of fs TA data.

T /K	τ_{ET2} / ps			$k_{ET2} \times 10^9 / \text{s}^{-1}$		
	1	2	3	1	2	3
300	330	500	690	3.0	2.0	1.5
280	420	570	740	2.4	1.8	1.4
270	580	940	860	1.7	1.1	1.2
260	710	1000	850	1.4	1.0	1.2
250	770	1270	920	1.3	0.8	1.1
240	890	– ^a	940	1.1	– ^a	1.1
230	– ^b	1620	1000	– ^b	0.6	1.0

^a fs TA data for **2** at 240 K were not collected. ^b The data for **1** at 230 K is not included here because of the changed TA spectral features, see Figure S3.

Summary of theoretical estimation for *ET2*

Table S2. Summary of the estimated temperature dependent dielectric constant (ϵ) and refractive index (n) of dichloromethane as well as reorganization energy (λ_{ET2}), driving force ($-\Delta G_{ET2}$), activation energy (ΔG_{ET2}^\ddagger) associated with the second electron transfer in triad **1**.

T / K	ϵ	n	λ_{ET2} / eV	$-\Delta G_{ET2}$ / eV	ΔG_{ET2}^\ddagger / eV
300	8.7558	1.4210	0.668	0.559	0.004
270	9.9861	1.4380	0.672	0.569	0.004
250	11.0458	1.4493	0.675	0.576	0.004
230	12.2969	1.4606	0.678	0.582	0.003

Table S3. Summary of the calculated temperature dependent dielectric constant (ϵ) and refractive index (n) of solvent dichloromethane as well as reorganization energy (λ_{ET2}), driving force ($-\Delta G_{ET2}$), activation energy (ΔG_{ET2}^\ddagger) associated with the second electron transfer in triad **2**.

T / K	ϵ	n	λ_{ET2} / eV	$-\Delta G_{ET2}$ / eV	ΔG_{ET2}^\ddagger / eV
300	8.7558	1.4210	0.847	0.431	0.051
270	9.9861	1.4380	0.852	0.443	0.049
250	11.0458	1.4493	0.856	0.451	0.048
230	12.2969	1.4606	0.859	0.459	0.047

Table S4. Summary of the calculated temperature dependent dielectric constant (ϵ) and refractive index (n) of solvent dichloromethane as well as reorganization energy (λ_{ET2}), driving force ($-\Delta G_{ET2}$), activation energy (ΔG_{ET2}^\ddagger) associated with the second electron transfer in triad **3**.

T / K	ϵ	n	λ_{ET2} / eV	$-\Delta G_{ET2}$ / eV	ΔG_{ET2}^\ddagger / eV
300	8.7558	1.4210	0.995	0.403	0.088
270	9.9861	1.4380	1.001	0.418	0.085
250	11.0458	1.4493	1.006	0.428	0.083
230	12.2969	1.4606	1.010	0.437	0.081

The influence of temperature on solvent dielectric properties, *i.e.* dielectric constant ϵ and refractive index n , which may change λ (eq S1-2) and $-\Delta G_{\text{ET}}$ (eq S3-6), is considered in this work. It should be noted that the single linear relation indicated by the Marcus equation in the main text can really be expected when both λ and the term $(\lambda+\Delta G)^2/4\lambda$ (*i.e.* activation energy, $\Delta G_{\text{ET}}^\ddagger$) are temperature independent.¹³ Otherwise, deviation from single linear regression would be observed because of the impact of temperature on solvent dielectric properties.¹³ The previous study has shown that for the first electron transfer process both λ and $\Delta G_{\text{ET}}^\ddagger$ are insensitive to temperature change.¹² For the second electron transfer, according to Table S2-4, λ and $\Delta G_{\text{ET}}^\ddagger$ are constant with temperature which show maximum changes smaller than 2% and 8%, respectively. Hence, we conclude that the solvent itself would not cause significant deviations due to temperature change.

Temperature dependence of ETI

Table S5. Temperature dependence of time constants and the corresponding rate constants for the second electron transfer process (k_{ETI}) in **1–3** obtained from the global fit of fs TA data.

T / K	τ_{ETI} / ps			$k_{ETI} \times 10^{11} / \text{s}^{-1}$		
	1	2	3	1	2	3
300	2.0	3.8	3.0	5.0	2.6	2.7
280	2.2	3.2	6.0	4.5	3.1	1.7
270	2.5	5.0	6.7	4.0	2.0	1.5
260	3.2	5.3	7.6	3.1	1.9	1.3
250	2.9	4.7	9.0	3.4	2.1	1.1
240	3.5	–	10	2.9	–	1.0
230	–	6.0	14	–	1.7	0.7

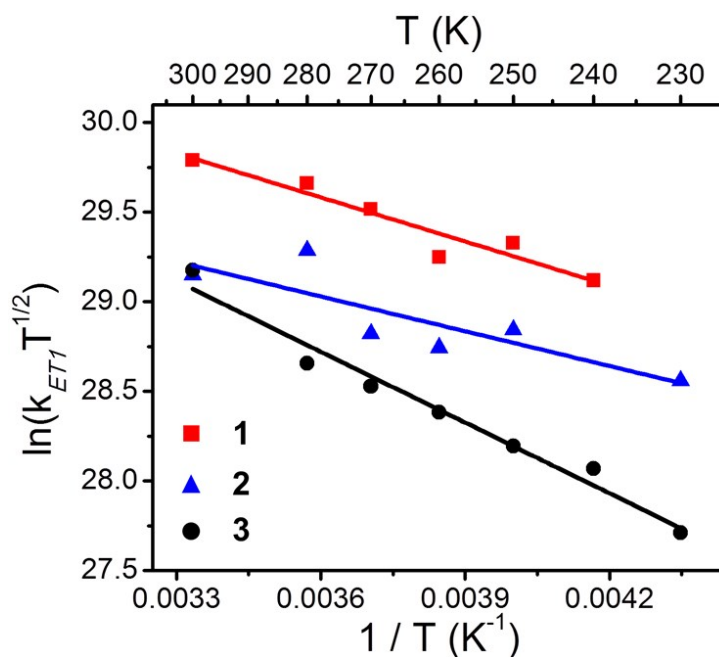


Figure S8. Plots of $\ln(k_{ETI} \cdot T^{1/2})$ vs. $1/T$ for the first electron transfer process ETI in **1** (red square), **2** (blue triangle) and **3** (black circle) with the corresponding linear fit according to eqn. (2).

Table S6. Summary of driving force ($-\Delta G$), reorganization energy (λ), electronic coupling (H_{DA}) and activation energy (ΔG^\ddagger) obtained from the experimental results for *ETI* in **1–3**.

	1	2	3
$-\Delta G / \text{eV}$	0.23	0.26	0.24
λ / eV	0.67	0.63	0.86
H_{DA} / cm^{-1}	157	86	265
$\Delta G^\ddagger / \text{eV}$	0.07	0.05	0.1

Concerning the *ETI* (temperature dependence of k_{ETI} see Figure S8) for which identical PTZ donor, donor-acceptor distance and chemical linkage are involved, Table S6 indicates very similar $-\Delta G$ values for **1–3** which vary by only 10% from 0.26 (**2**) to 0.23 (**1**). Likewise, λ is rather similar for **1** (0.67 eV) and **2** (0.63 eV). However, for **3** λ is approximately 36% larger (0.86 eV). Noteworthy, H_{DA} values are quite different amongst the investigated triads. H_{DA} decreases in the order **3** (265 cm^{-1}) > **1** (157 cm^{-1}) > **2** (86 cm^{-1}). This observation can be rationalized by the different substitution on the tpy- C_{60} ligand.¹² Similar results have recently been reported in structurally related dyad systems.¹² The variations in λ and H_{DA} amongst the triads can be rationalized by considering the electron-rich $-\text{OC}_8\text{H}_{17}$ groups in **3**. They indirectly increase the electron density at the photoactive Ru(tpy)₂-core and increase λ and H_{DA} .¹² **1** and **2** on the other hand contain pure electron-withdrawing substituents on the tpy- C_{60} ligand, the electronic effect of which apparently decrease the electronic coupling underlying *ETI*.¹²

REFERENCES

1. Y. Luo, K. Barthelmes, M. Wächtler, A. Winter, U. S. Schubert and B. Dietzek, *Chem. Eur. J.*, 2017, **23**, 4917–4922.
2. Y. Luo, K. Barthelmes, M. Wächtler, A. Winter, U. S. Schubert and B. Dietzek, *J. Phys. Chem. C*, 2017, **121**, 9220–9229.
3. K. Barthelmes, A. Winter and U. S. Schubert, *Eur. J. Inorg. Chem.*, 2016, 5132–5142.
4. M. Wächtler, J. Kübel, K. Barthelmes, A. Winter, A. Schmiedel, T. Pascher, C. Lambert, U. S. Schubert and B. Dietzek, *Phys. Chem. Chem. Phys.*, 2016, **18**, 2350–2360.
5. R. A. Marcus and N. Sutin, *Biochim. Biophys. Acta*, 1985, **811**, 265–322.
6. M. Kuss-Petermann and O. S. Wenger, *Phys. Chem. Chem. Phys.*, 2016, **18**, 18657–18664.
7. E. Göransson, J. Boixel, J. Fortage, D. Jacquemin, H.-C. Becker, E. Blart, L. Hammarström and F. Odobel, *Inorg. Chem.*, 2012, **51**, 11500–11512.
8. J. Kroon, H. Oevering, J. W. Verhoeven, J. M. Warman, A. M. Oliver, M. N. Paddon-Row, *J. Phys. Chem.*, 1993, **97**, 5065–5069.
9. P. Vath, M. B. Zimmt, D. V. Matyushov, G. A. Voth, *J. Phys. Chem. B*, 1999, **103**, 9130–9140.
10. D. R. Lide, editor in chief. *Handbook of Chemistry and Physics*, 84th edition.
11. H. Shekaari, A. Bezaatpour and A. Soltanpour, *J. Chem. Eng. Data*, 2010, **55**, 5927–5931.
12. Y. Luo, J. H. Tran, M. Wächtler, M. Schulz, K. Barthelmes, A. Winter, S. Rau, U. S. Schubert and B. Dietzek, *Chem. Commun.*, 2019, **55**, 2273–2276.
13. J. Kroon, H. Oevering, J. W. Verhoeven, J. M. Warman, A. M. Oliver and M. N. Paddon-Row, *J. Phys. Chem.*, 1993, **97**, 5065–5069.